Electronic Supplementary Material (ESI) for Inorganic Chemistry Frontiers.

## Electronic Supplementary Information:

# A dual-function battery for desalination and energy storage

Liubin Wang, Chaonan Mu, Haixia Li, and Fujun Li*

Key Laboratory of Advanced Energy Materials Chemistry (Ministry of Education), College of Chemistry, Nankai University, Tianjin 300071, P. R. China

*E-mail: fujunli@nankai.edu.cn

## 1. Experimental Section

***Material Synthesis*****:** The NTP was prepared by a solid-state synthesis method. In a typical process, $NaH_2PO_4 \cdot 2H_2O$ (10.2 mmol, Aladdin.), $TiO_2$ (20 mmol, anatase, 99.8% metals basis, 5 ~ 10 nm Aladdin.), $(NH_4)_2HPO_4$ (19.8 mmol, 99.9%, Aladdin.), and 400 mg carbon nanotube (CNano Technology Ltd.) were ball-milled in a planetary ball mill (QM-3SP2) at 400 rpm for 24 h. The mixture were pre-calcined at 400 $^{o}$C for 2 h in the flowing $H_2$/Ar (5 vol% $H_2$), followed by reground in an agate mortar and calcination at 850 $^{o}$C for another 10 h. The Ag foil (99.9 wt% purity, with a thickness of 50 μm) was purchased from Qingyuan metal material Co. Ltd.. It was washed with hydrochloric acid and subsequently with deionized water and ethanol for several times to remove surface impurities before use.

***Material Characterization:*** XRD patterns were obtained on a Rigaku SmartLab (Cu Kα radiation). EDS elemental mappings and elemental analyses were conducted on a JEOL JSM-7500F microscope (operating voltage, 5 kV) equipped with an EDS analyzer (operating voltage, 20 kV). IR spectra were collected using Fourier transform infrared spectroscopy (FTIR, Bruker Tensor II Sample Compartment RT-DLaTGS). Raman spectra were obtained on a confocal Raman microscope (DXR, Thermo-Fisher Scientific) with an argon-ion laser of 633 nm in ambient air. TEM and HRTEM images were obtained on JEOL 2100F. The thermal stability and CNTs content were estimated by TG-DSC analyzer (TG209 DSC204 DMA242 TMA202). XPS was conducted on a Perkin Elmer PHI 1600 ESCA system to characterize the intermediates in the discharge and charge process.

***Electrochemical Measurements*****:** The anode was prepared by blending the NTP, Super P and PVDF with a mass ratio of 8:1:1. The as-prepared slurry was pasted onto a carbon paper and dried in a vacuum oven at 100 °C for 10 h. The electrode for the in-situ XRD battery was prepared with by mixing NTP, Super P and PTFE onto a stainless steel current collector. The three-electrode cells were composed of a saturated calomel electrode as reference electrode, platinum foil as counter electrode, and the NTP anode or Ag cathode as working electrode, respectively, in the 1.0 M of NaCl aqueous solution. The CV tests of the three-electrode cells and full batteries were carried out on Solartron 1470E (AMETEK). The NTP/Ag battery was assembled in CR2032 coin cells with Whatman glass microfiber as separator and 100 μL of 1.0 M of NaCl aqueous electrolyte. EIS data were obtained on Solartron 1470E (AMETEK) at open-circuit voltage with a voltage amplitude of 5.0 mV over the frequency range from 100 kHz to 100 mHz. Galvanostatic charge/discharge measurements were carried out on Land instrument (CT2001A). The solar cell was purchased from Crab kingdom mall. The ionic conductivity was tested on a conductivity meter (DDSJ-308A, Shanghai INESA & Scientific Instrument Co. Ltd.). For monitoring concentration change of the electrolyte during photocharge and discharge process, the electrolyte was diluted for 100 times. All the electrochemical tests were performed at room temperature.

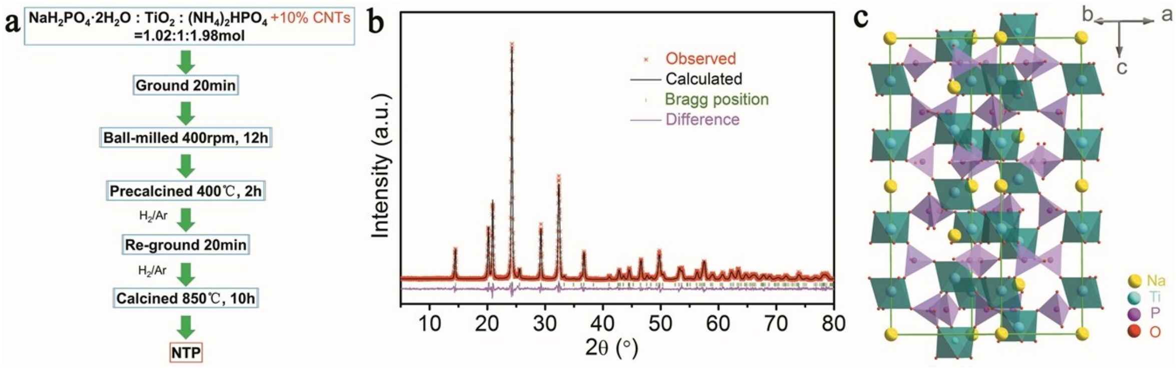

**Figure S1**. (a) Preparation process of the NTP; (b) powder XRD pattern and its Rietveld refinement (red dots: obtained data; black line: calculated data; olive bars: bragg position; magenta line: difference curve) of the NTP; and (c) crystal structure of $NaTi_2(PO_4)_3$. XRD pattern and its Rietveld refinement in Figure S1b reveal the high purity of the as-prepared NTP.

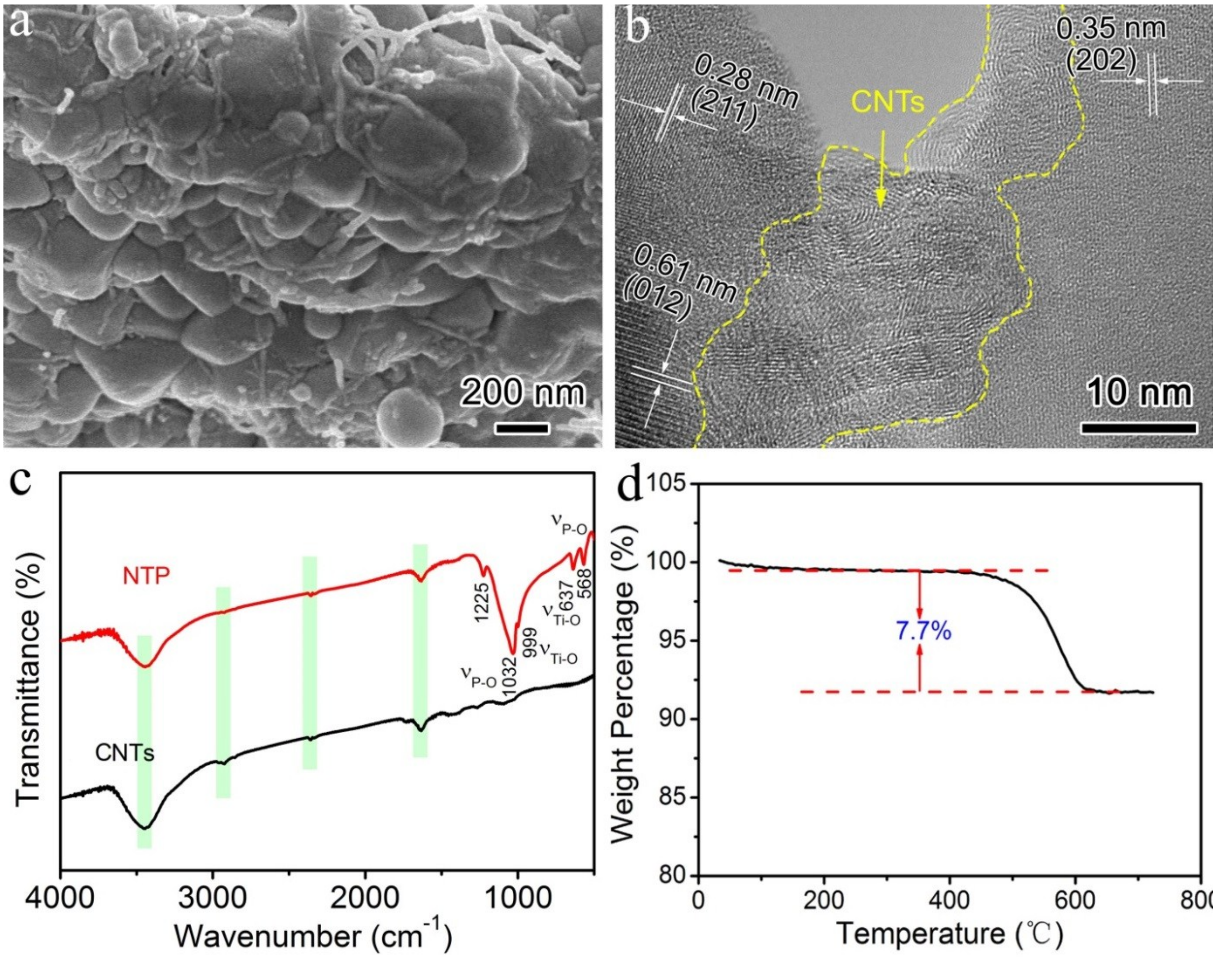

**Figure S2**. (a) SEM image; (b) high-resolution TEM image; (c) IR spectra; and (d) thermogravimetric analysis of the NTP.

Figure S2a and b show the SEM and TEM images of the NTP, respectively. The NTP particles are well connected by the CNTs, providing a good conductive network for electron conduction. Figure S2c displays the FTIR spectra of the prepared NTP and CNTs. The vibrations from P-O bonds of $PO_4$ tetrahedrons are evident at 1032 and 568 cm$^{-1}$. The bonds at 637 and 999 cm$^{-1}$ can be ascribed to the Ti-O bonds in $TiO_6$ octahedra. The other bonds can be well matched with the spectrum of CNTs. Based on the thermogravimetric analysis, the mass of CNTs in the NTP compound is estimated to be 7.7%.

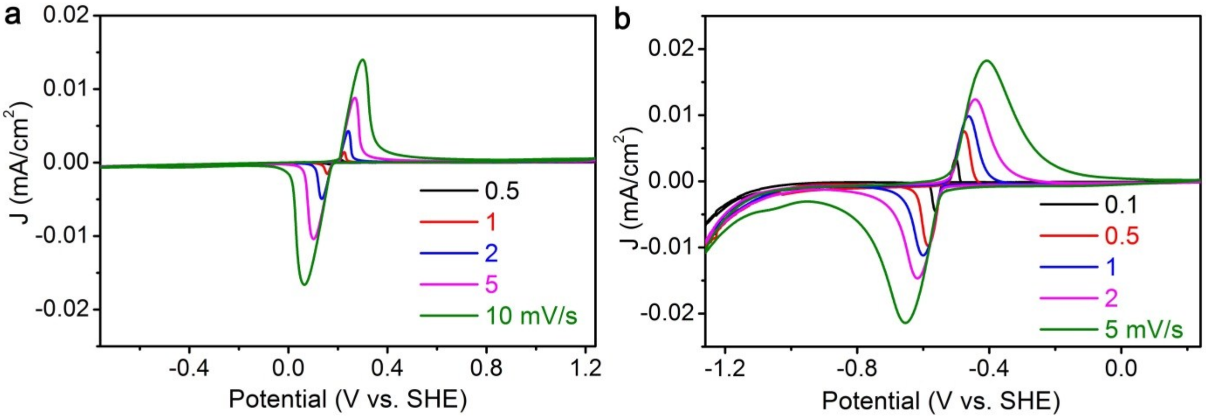

**Figure S3**. CV curves of Ag (a) and NTP (b) as working electrode in three-electrode cells in 1.0 M of NaCl aqueous electrolyte at different scan rates. Counter electrode, platinum foil (Pt), and reference electrode, saturated calomel electrode.

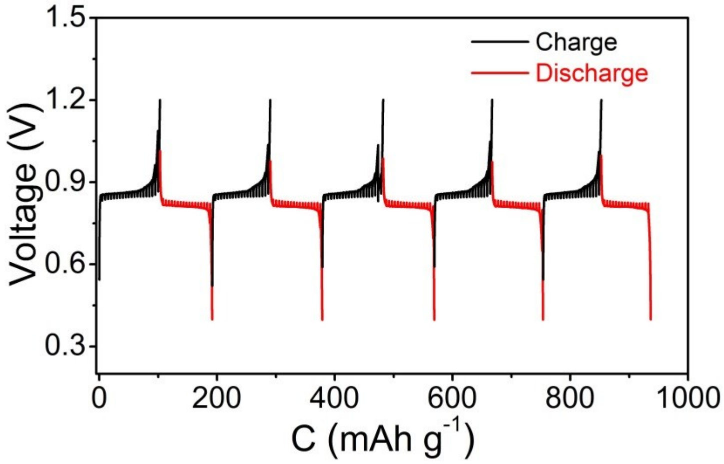

**Figure S4**. Galvanostatic intermittent titration technique (GITT) profiles of the NTP/Ag battery (charge/discharge, 3 minutes; rest, 15 minutes; current density, 1 C ).

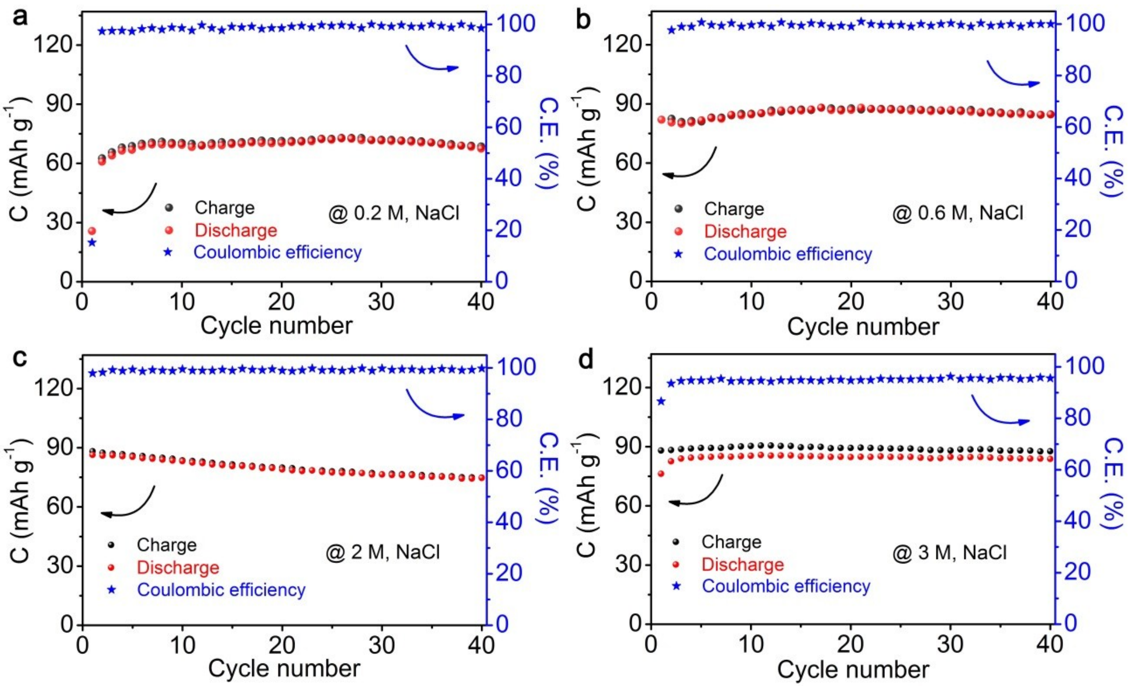

**Figure S5.** Electrochemical performance of NTP/Ag battery at 1C in different electrolytes: (a) 0.2 M, NaCl; (b) 0.6 M, NaCl; (c) 2 M, NaCl; (d) 3 M, NaCl.

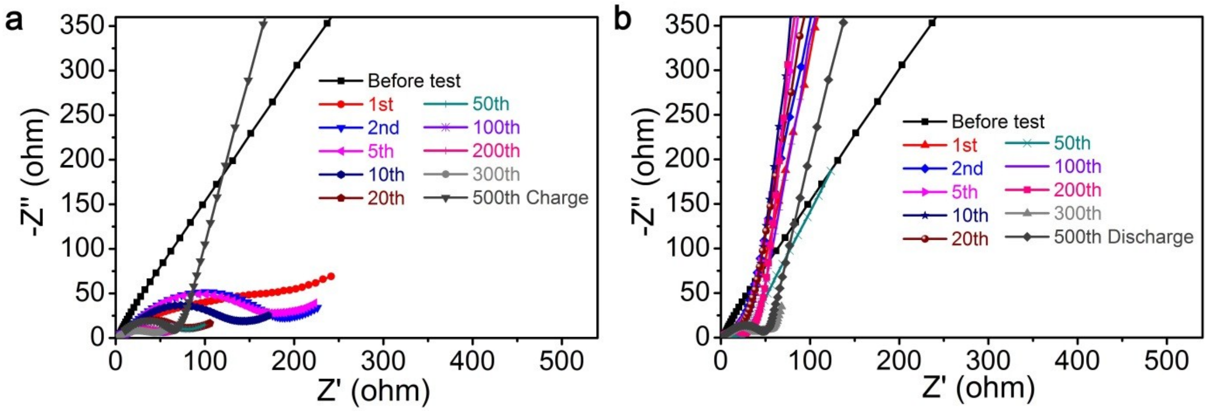

**Figure S6.** EIS spectra of NTP/Ag battery after charge (a) and discharge (b) during varied cycles, respectively.

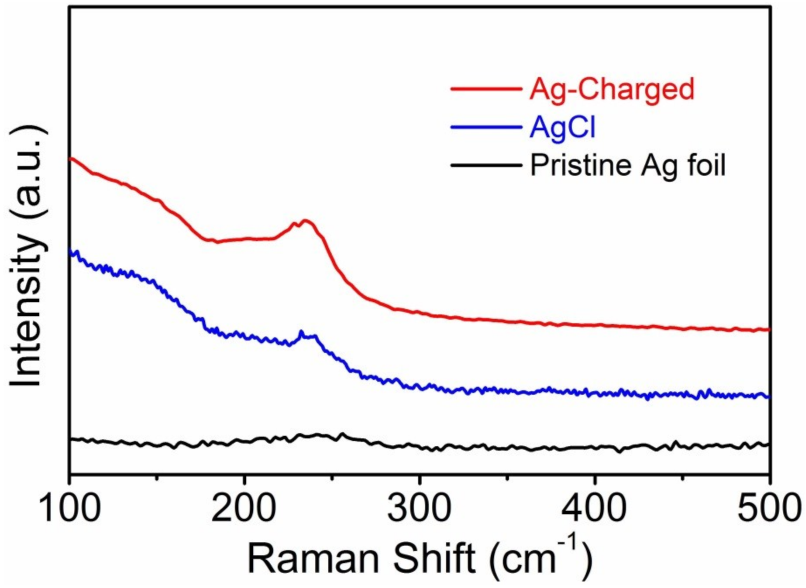

**Figure S7**. Raman spectra of the pristine Ag foil, AgCl, and the charged Ag electrode.

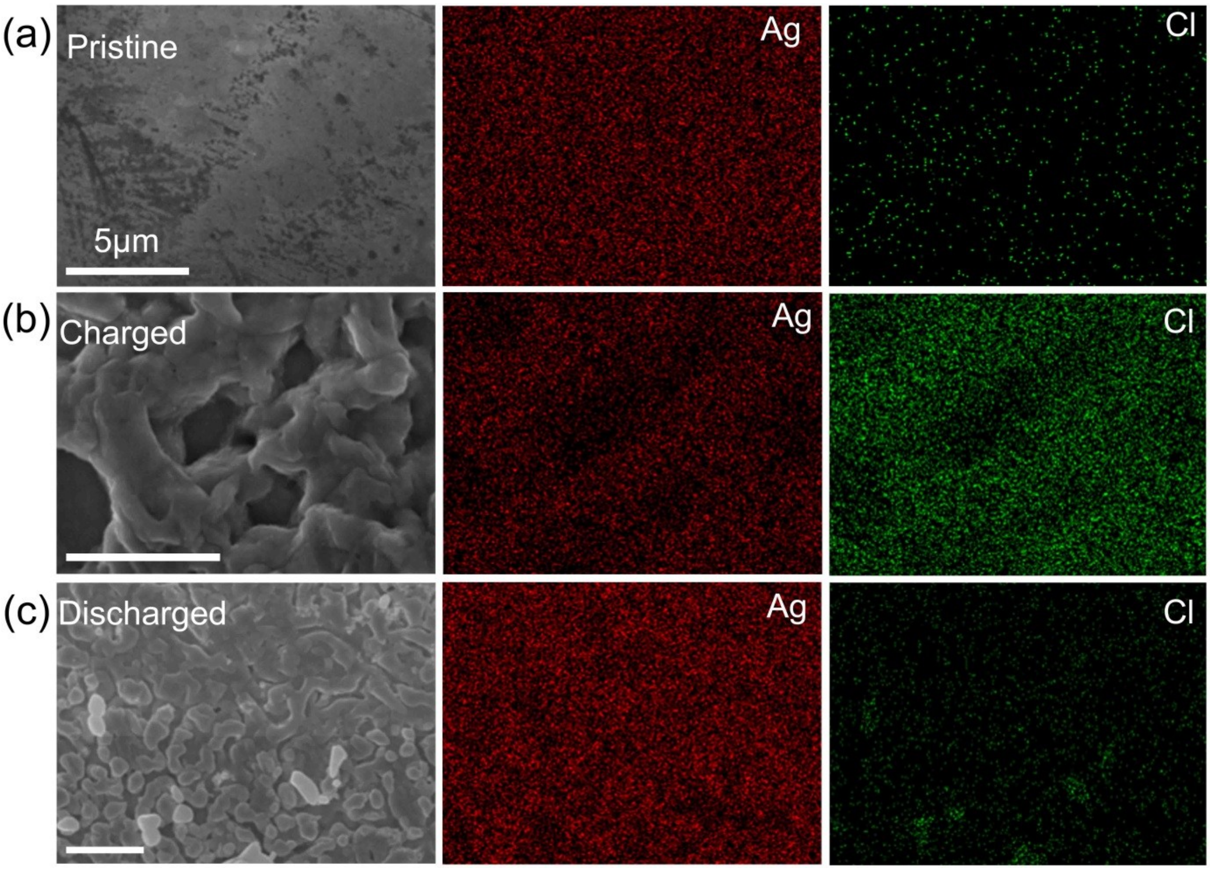

**Figure S8**. SEM images and EDS mappings of Ag and Cl in the different Ag electrodes: (a) the pristine electrode, and (b) charged and (c) discharged electrode in the 1st cycle.

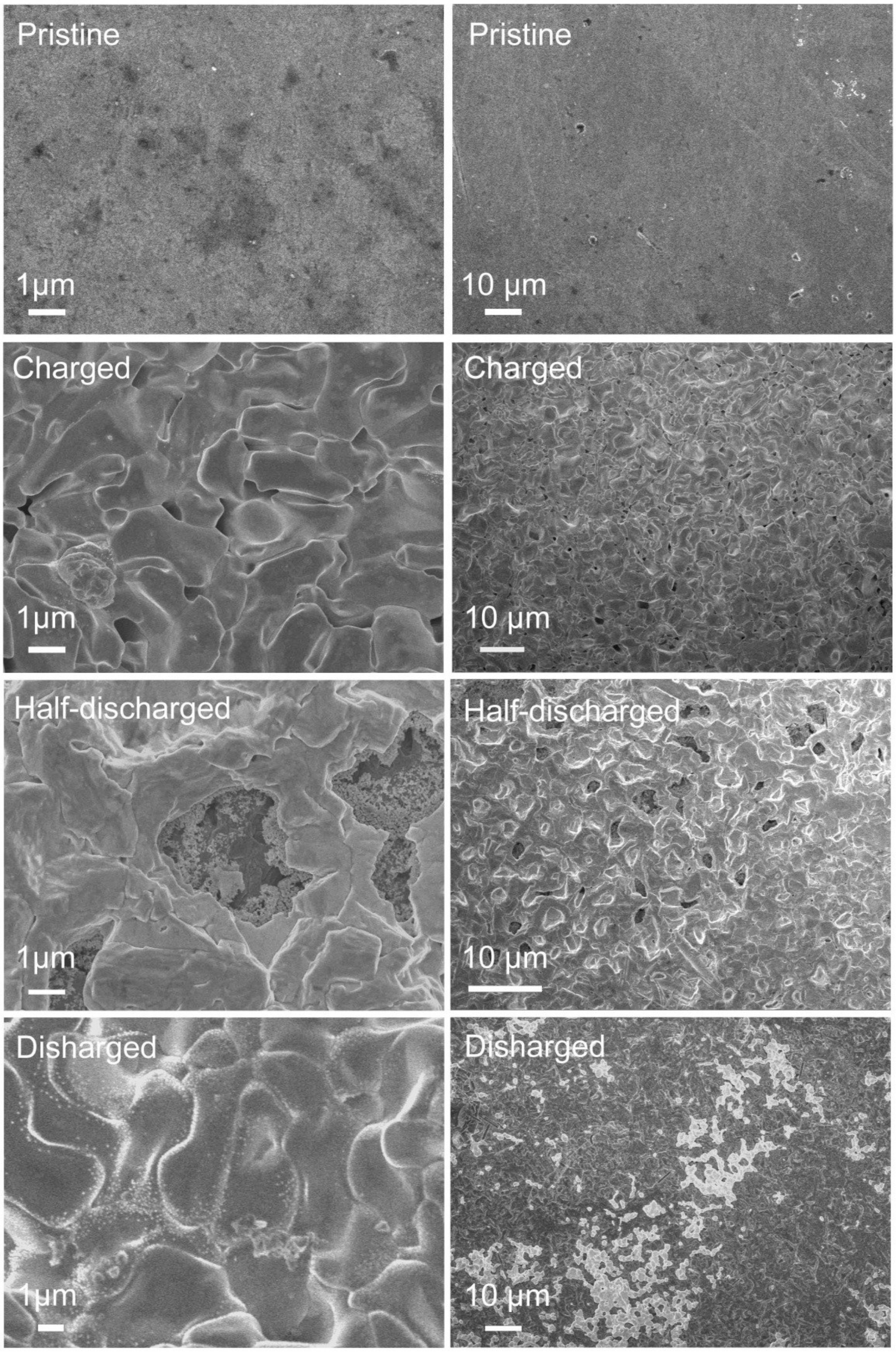

**Figure S9**. SEM images of the pristine, discharged, half discharged and fully discharged Ag electrodes.

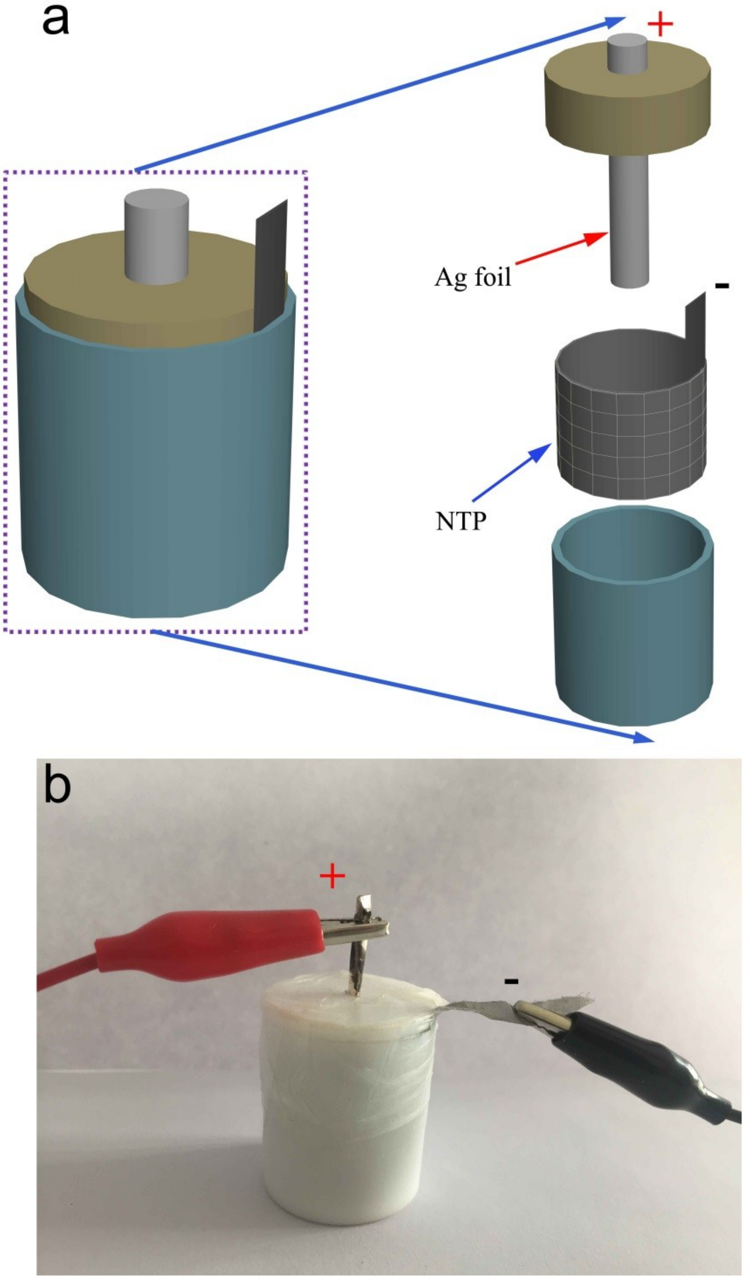

**Figure S10**. (a) Schematic configuration and (b) photograph of the dual-function battery .

**Figure S11**. Open-circuit voltage of the solar cell.

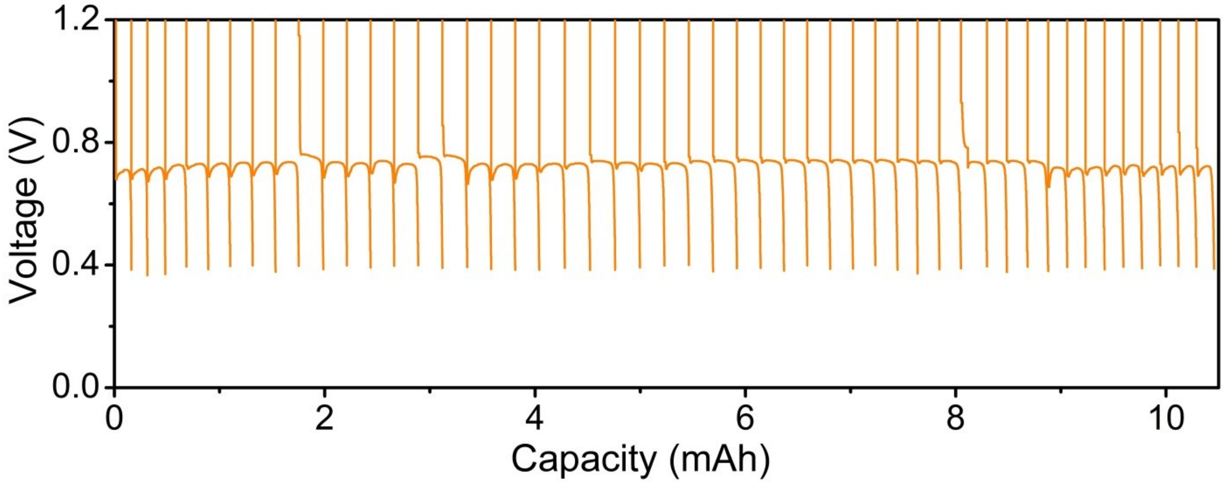

**Figure S12**. Discharge profiles of the dual-function battery after photocharge.

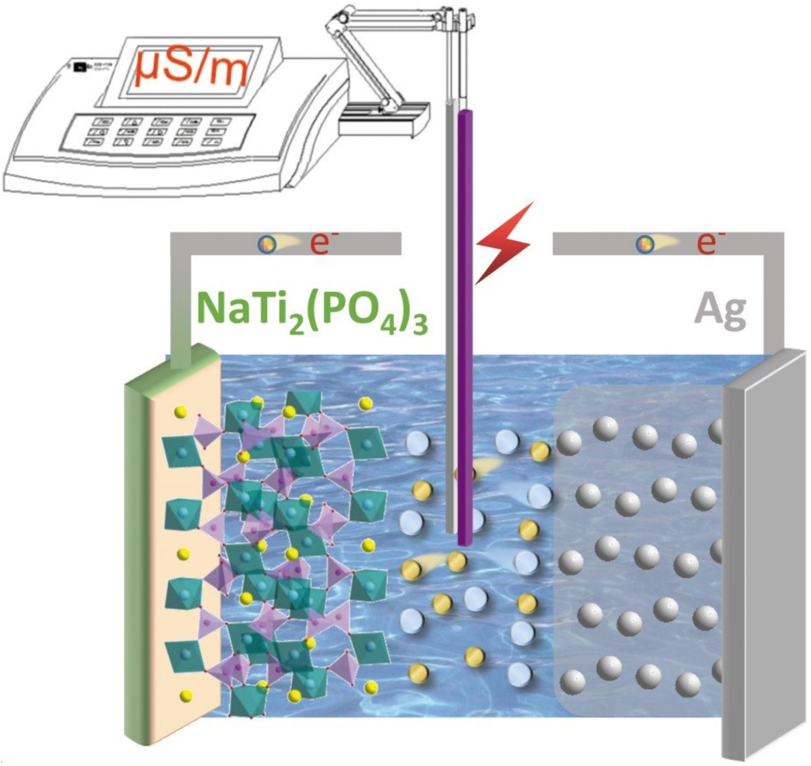

**Figure S13**. Schematic illustration of conductivity measurement of electrolyte in the dual-function battery.

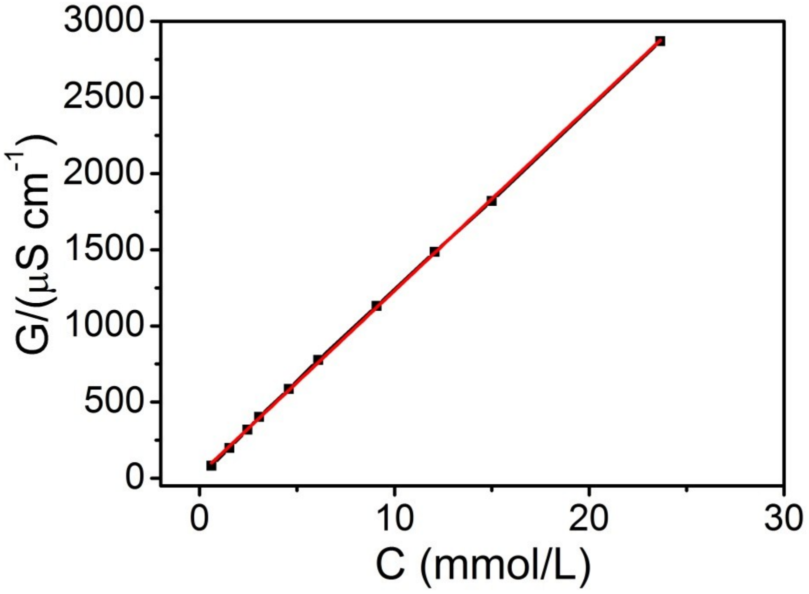

**Figure S14**. Relationship between ion conductivity and concentration of the NaCl aqueous solution.

**Table S1** Comparison of the salt adsorption capacity (SAC) in different desalination batteries.

| System | Discharge voltage (V) | Current density (mA $g^{-1}$) | Capacity (mAh $g^{-1}$) | NaCl (M) | SAC (mg $g^{-1}$) | Reference |
|---|---|---|---|---|---|---|
| NTP/Ag | 0.72 | 1000 | $70_{NTP}$ | 1 | 151.5 | This work |
| Ag/$MnO_2$ | 0.3 | \ | \ | 0.6 | \ | 1 |
| BiOCl/$Na_{0.44}MnO_2$ | \ | 100 | $95.8_{BiOCl}$ | 1 | 86.6 | 2 |
| AgCl/$Na_{0.44}MnO_2$ | \ | 100 | $72.2_{AgCl}$ | 0.015 | 86.1 | 3 |
| $NaTi_2(PO_4)_3$/Bi | 0.55 | 66.7 | full | 0.6 | 82.9 | 4 |
| $TiS_2$/K20 | 0.4 | 100 | $60_{TiS2}$ | 0.6 | 14.5 | 5 |
| $NaTi_2(PO_4)_3$/AgNPs | \ | 100 | None$\backslash_{NaTi2(PO4)3}$ | \ | 53.7 | 6 |

The SAC was calculated based on the active mass of anode or cathode, which is marked at the right subscript in the column of capacity. The specific charge capacity of $NaTi_2(PO_4)_3$, $Na_{0.44}MnO_2$, Ag and BiOCl is~133, ~35, ~92 and ~248 mAh $g^{-1}$, respectively.[6]

Reference

1. M. Pasta, C. D. Wessells, Y. Cui, F. La Mantia, *Nano Lett.,* 2012, **12**, 839-843.
2. F. Chen, Y. Huang, L. Guo, L. Sun, Y. Wang, H. Y. Yang, *Energy Environ. Sci.,* 2017, **10**, 2081-2089.
3. F. Chen, Y. Huang, L. Guo, M. Ding, H. Y. Yang, *Nanoscale,* 2017, **9**, 10101-10108.
4. D. Nam, K. Choi, *J. Am. Chem. Soc.,* 2017, **139**, 11055-11063.
5. P. Srimuk, J. Lee, A. Tolosa, C. Kim, M. Aslan, V. Presser, *Chem. Mater.,* 2017, **29**, 9964-9973.
6. Y. Huang, F. Chen, L. Guo, J. Zhang, T. Chen, H. Y. Yang, *Desalination*, 2018, https://doi.org/10.1016/j.desal.2018.02.006.